VARIATIONS IN THE ELECTRICAL SHORT-CIRCUIT CURRENT DECAY FOR RECOMBINATION LIFETIME AND VELOCITY MEASUREMENTS

TAE-WON JUNG*, FREDRIK A. LINDHOLM and ARNOST NEUGROSCHEL

Department of Electrical Engineering, University of Florida, Gainesville, FL 32611 (U.S.A.)

(Received July 10, 1986; accepted in revised form January 9, 1987)

Summary

An improved measurement system for electrical short-circuit current decay is presented that extends applicability of the method to silicon solar cells having an effective lifetime as low as 1 μs. The system uses metal/oxide/semiconductor transistors as voltage-controlled switches. Advances in theory developed here increase precision and sensitivity in the determination of the minority-carrier recombination lifetime and recombination velocity. A variation of the method, which exploits measurements made on related back-surface field and back-ohmic contact devices, further improves precision and sensitivity. The improvements are illustrated by application to 15 different silicon solar cells.

1. Introduction

This paper describes various improvements of the method of electrical short-circuit current decay (ESCCD) [1] for measuring the recombination lifetime and velocity of p–n junction solar cells. Firstly, the switching circuit in ref. 1 has been improved to accommodate decay time constants down to the submicrosecond range. We used metal/oxide/semiconductor transistors to provide a voltage-controlled switch between the two terminals of a solar cell. This use yields a much faster switching time and a simpler circuit in comparison with the bipolar circuit of ref. 1.

Secondly, in the previous work [1], we used the initial amplitude of the first-mode current $i_{\text{first-mode}}(0^+)$ of the transient together with the initial slope, the decay time constant τ_d, as the ESCCD parameters used to determine the recombination lifetime τ and the back-surface recombination velocity S (see Appendix A). The parameter $i_{\text{first-mode}}(0^+)$ is proportional

*Dr. Jung is now with the Harris Semiconductor Corporation, Melbourne, FL, U.S.A.

0379-6787/87/$3.50

to $\exp\{eV(0^-)/kT\}$ where $V(0^-)$ is the difference between the voltage at the terminals at $t = 0^-$ and the voltage drop in the series resistance. Thus, in the method of ref. 1, τ and S are determined by three measurable parameters: $i_{\text{first-mode}}(0^+)$, τ_d and $V(0^-)$. The last of these is the least accurately determined of the three because of possible contact and cell series resistances. In the improved approach of this paper we eliminate the need to measure $V(0^-)$ by treating $i_{\text{first-mode}}(0^+)/I_F(0^-)$ as the measurable parameter. In the ratio the factor $\exp\{eV(0^-)/kT\}$ cancels out.

Thirdly, we consider the sensitivity problem involved in the method of ESCCD for thin or thick solar cells. By a thin solar cell, for example, we mean that the thickness of its base region is much less than the diffusion length. We analyze this problem by using the $S(\tau)$ locus for a given measured decay time constant. For a thin solar cell, we introduce new performance parameters, $S_{\max}$, $\tau_{\min}$ and R_M, the importance of which is discussed in this paper.

Fourthly, we show quantitatively that the electrical short-circuit current decay curve is not affected by either the series resistance or the shunt resistance of the usual solar cell.

Fifthly, we note that the use of I_{FO} in the ratio above brings the emitter recombination current I_{QNE} into our method for determining τ and S of the base region. This, however, is only apparently a problem. Indeed, we illustrate that use of the $S(\tau)$ locus enables a determination of I_{QNE}, thus enhancing the utility of the method to be described.

Finally, we present a new method in which ESCCD applied to a back-surface field (BSF) solar cell and a nearly identical back-ohmic contact cell yields highly accurate values for S and τ.

2. Theory

2.1. Theory of the method of electrical short-circuit current decay

A general description of the theory and the underlying physics for the ESCCD method appeared in ref. 1. In this section we exploit advantages of the two-port network formulation introduced in ref. 1, the circuit representation for which is illustrated in Fig. 1. To illustrate the ideas, we have assumed a p^+–n–n^+ structure.

In this figure we have used the y parameter set of network theory [2]. This choice is arbitrary. Instead we could have chosen any of the four parameter sets. Mapping into the other three sets is straightforward and may be desirable, for example, for certain input excitations and output terminations. That is one advantage of a two-port network representation.

Other advantages include the following: (a) systematic determination of the natural frequencies [2]; (b) systematic conversion from transient to steady-state excitations, attained by setting the complex frequency variable s to zero; (c) systematic connections to the underlying physics, as we shall illustrate; (d) systematic treatment of various terminations and excitations;

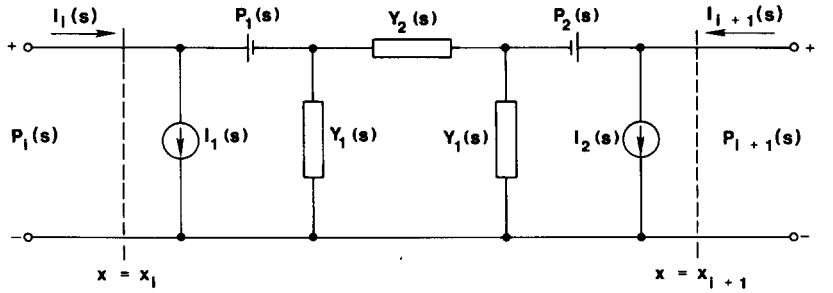

Fig. 1. Two-port network representation of an n-type quasi-neutral region with boundary conditions at $x = X_{QNB}$ and $x = 0$. The nodal variable is the excess minority carrier concentration. P_1, P_2, I_1, I_2 denote initial values.

(e) systematic derivation of the system function in the complex frequency domain, which maps into the impulse response (Green's function) in the time domain, an advantage which we will illustrate later by use of the Elmore definition of delay [3].

For the analysis of the ESCCD method for a solar cell (Fig. 1), we put a short-circuit path at $x = 0$ and a back contact having recombination velocity S at $x = X_{QNB}$ in the y parameter network representation. The boundary condition at $x = X_{QNB}$, $I(X_{QNB}, s) = AeSP(X_{QNB}, s)$, removes $I_2(s)$ and $P_2(s)$ in Fig. 1 from consideration. Figure 2 displays the resulting two-port network representation of the n-type quasi-neutral base region of a solar cell. Here

$$Y_s \equiv \frac{-I(X_{QNB}, s)}{P(X_{QNB}, s)} = AeS \tag{1}$$

Solving the network of Fig. 2 for $I(0, s)$ under the low-injection condition yields

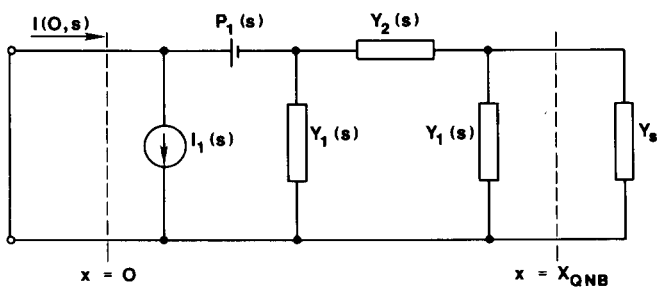

Fig. 2. Equivalent two-port network representation of a quasi-neutral base of a solar cell with a general contact at $x = X_{QNB}$ under short-circuit current decay condition. The excess minority carrier concentration at $x = 0$ vanishes.

$$I(0, s) = \frac{i(0, 0^-)}{s} - Y_1 \frac{p(0, 0^-)}{s} - \frac{(Y_1 + Y_s)Y_2}{Y_1 + Y_2 + Y_s} \frac{p(0, 0^-)}{s} \tag{2}$$

where

$$p(0, 0^-) = \frac{n_i^2}{N_{DD}} \left[\exp\left\{ \frac{eV(0^-)}{kT} \right\} - 1 \right]$$

and where

$$Y_1 = \frac{eD}{L_p^*} \left\{ \coth\left(\frac{X_{QNB}}{L_p^*} \right) - \operatorname{cosech}\left(\frac{X_{QNB}}{L_p^*} \right) \right\}$$

and

$$Y_2 = e(D_p/L_p^*) \operatorname{cosech}(X_{QNB}/L_p^*)$$

in which

$$L_p^* = \frac{D_p \tau_p}{(1 + s\tau_p)^{1/2}} \tag{3}$$

If we use the Cauchy residue theorem to obtain the inverse transform of $I(0, s)$, we get an infinite series for $i(0, t)$. Truncating this series after the first term, at $t = 0^+$, yields $i(0, t) \approx i_{\text{first-mode}}(0^+) \exp(-t/\tau_d)$, $t > \tau_d$,

$$i_{\text{first-mode}}(0^+) = I_{FMO} \left[\exp\left\{ \frac{eV(0^-)}{kT} \right\} - 1 \right] \tag{4}$$

where

$$I_{FMO} = \frac{AeDK_1 n_i^2}{s_1 L N_{DD}} \frac{\cot(K_1 X_{QNB}/L) - DK_1/LS}{(\tau/2K_1^2) + (X_{QNB}/2S) \operatorname{cosec}^2(K_1 X_{QNB}/L)} \tag{5}$$

The ESCCD decay time τ_d results from recombination at the back surface and in the volume of the base together with minority-carrier exiting from the base edge of the p–n junction space charge region.

The minority-carrier current at $x = 0$ for $t < 0$ is

$$i(0, 0^-) = I_{QNBO} \left[\exp\left\{ \frac{eV(0^-)}{kT} \right\} - 1 \right] \tag{6}$$

where

$$I_{QNBO} = \frac{ADn_i^2}{LN_{DD}} \frac{\sinh(X_{QNB}/L) + \alpha \cosh(X_{QNB}/L)}{\cosh(X_{QNB}/L) + \alpha \sinh(X_{QNB}/L)} \tag{7}$$

and where $\alpha = LS/D$. Here α is the ratio of the normalized surface recombination velocity to the diffusion velocity [4]. We form the ratio R

$$R \equiv \frac{I_{FMO}}{I_{QNBO}}$$

$$= \frac{2K_1}{S_1} \frac{\cot A_1 + \tan A_1}{(X_{QNB}/A_1)^2/D + (X_{QNB}/S)\,\mathrm{cosec}^2 A_1}$$

$$\times \frac{\cosh(X_{QNB}/L) + \alpha \sinh(X_{QNB}/L)}{\sinh(X_{QNB}/L) + \alpha \cosh(X_{QNB}/L)} \tag{8}$$

where $A_1 = K_1 X_{QNB}/L$ and where K_1 and A_1 are obtained by solving eqn. (B3) of Appendix B of ref. 1. The ratio R will be utilized for the determination of the quasi-neutral base parameters.

2.2. Dark current–voltage characteristic of a solar cell

The equivalent circuit of a solar cell in the dark condition, including series and shunt resistances, is shown in Fig. 3. If we assume that the space-charge recombination current component is negligible [5], the current–voltage (I–V) characteristic of the solar cell is

$$I = I_D + I_{sh} \tag{9}$$

$$= I_{FO}\left\{\exp\left(\frac{eV}{kT}\right) - 1\right\} + \frac{V}{r_{sh}} \tag{10}$$

Here I_{FO} is the pre-exponential factor of the forward bias current and V is the voltage across the space-charge region. The pre-exponential factor I_{FO} in eqn. (9) has two components

$$I_{FO} = I_{QNBO} + I_{QNEO} \tag{11}$$

where I_{QNBO} is the quasi-neutral-base current component and I_{QNEO} is the quasi-neutral-emitter current component.

The voltage across the two terminals of the solar cell V_{out} is

$$V_{out} = Ir_s + V \tag{12}$$

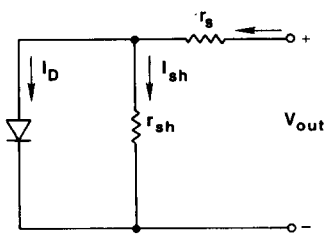

Fig. 3. A simple diode model with series resistance and shunt resistance in the dark condition.

As the forward bias increases, the current I in eqn. (9) becomes more dominated by the component I_D and the effect of I_{sh} becomes negligible

$$I \approx I_{FO} \exp\left(\frac{eV}{kT}\right) \tag{13}$$

Combining eqns. (12) and (13), we obtain an expression for V_{out} in terms of I, r_s and I_{FO}

$$V_{out} = r_s I + \frac{kT}{q} \ln\left(\frac{I}{I_{FO}}\right) \tag{14}$$

There are two unknowns, r_s and I_{FO}, in eqn. (14). We estimate r_s and I_{FO} by measuring the dark or illuminated I–V characteristics in the standard manner. The pre-exponential factor I_{FO} will be utilized for the determination of the base material parameters.

2.3. Combined method of electrical short-circuit current decay and dark current–voltage characteristic

In this section, we present a method for the determination of the parameters of a solar cell. This method involves combining the ESCCD and dark I–V characteristic methods. Using the ESCCD method, we measure the decaying time constant of the first mode τ_d and the ratio R_M of the currents in eqns. (4) and (10) neglecting V/r_{sh} in eqn. (10)

$$R_M \equiv \frac{I_{FMO}}{I_{FO}} \tag{15}$$

in which the subscript FMO refers to the pre-exponential factor of the first-mode current. Using the dark I–V measurement, we estimate the pre-exponential factor I_{FO} by eliminating the series resistance effect as described in Section 2.2.

From the measured value of τ_d, one can generate an $S(\tau)$ locus on the τ–S plane using Appendix B, eqn. (B3) of ref. 1; each point on this locus must produce the measured value of τ_d. Each point (τ, S) also has its own value of the ratio R, defined in eqn. (8), since R is a function of both τ and S. Also, each point (τ, S) produces its own value for I_{QNBO} of eqn. (7).

Now we have three equations for three unknowns. The three unknowns are τ, S and I_{QNEO} and the three equations are

$$\tau_d = f_1(\tau, S) \qquad \text{(B3 of ref. 1)}$$

$$I_{FO} = f_2(\tau, S, I_{QNEO}) \tag{11}$$

$$R_M = f_3(\tau, S, I_{QNEO}) \tag{15}$$

Using these equations and the measured values of their left-hand sides, one can solve for τ, S and I_{QNEO} in a manner to be described later.

3. Experiments

3.1. Improvements in the circuit for electrical short-circuit current decay

Previously we used a bipolar-transistor switching circuit in ref. 1 to measure the decay time constant and the initial amplitude of the first natural-frequency current at $t = 0^+$. We have made this switching circuit faster and simpler by replacing bipolar transistors by power metal/oxide/semiconductor field effect transistor (MOSFET) switches.

To increase speed further, we reduced the parasitic effects existing in the measurement circuit. To decrease the parasitic inductance, we shortened the discharge path of the stored carriers and also shortened the length of the probes of the oscilloscope.

The improved circuit is illustrated in Fig. 4. In this circuit the power MOSFET switch has a turn-on resistance of 0.6 Ω. The input capacitance of the MOSFET is 250 pF. The output impedance of the pulse generator is 50 Ω. The turn-on switching time of this measurement circuit is 12.5 ns (250 pF × 50 Ω). Thus the speed of the measurement circuit is adequate for any bipolar devices having τ_d larger than 100 ns. This switching circuit provides a sudden shorted path across the two terminals of a solar cell in a manner similar to that of the bipolar switching circuit described in ref. 1.

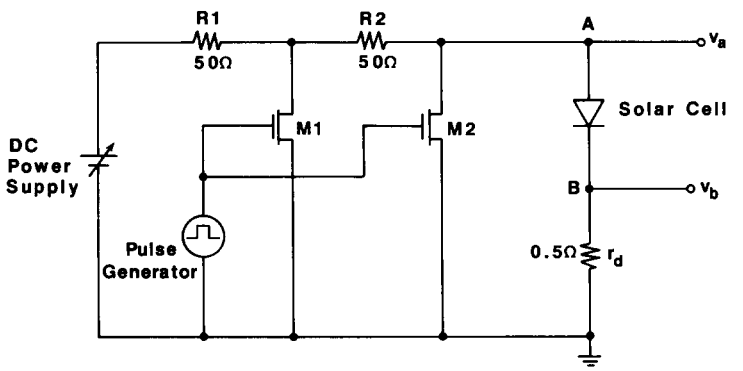

Fig. 4. Switching circuit used in measuring short-circuit current decay parameters, τ and S.

3.2. Quality of the short circuit of the switching circuit

We now consider the quality of short circuit provided by the switching circuit of Fig. 4. The discharging path has a series resistance of a few ohms instead of being a perfect short circuit. The voltage across the junction space-charge region does not vanish as long as the current flows through the series resistance. Figure 5 displays the equivalent circuit during discharge when the first-term natural-frequency current dominates the discharging current. Higher-term natural-frequency current components have vanished previously from the equivalent circuit representation of Fig. 5 since they have shorter decay time constants than the time constant τ_d of the first-term natural-

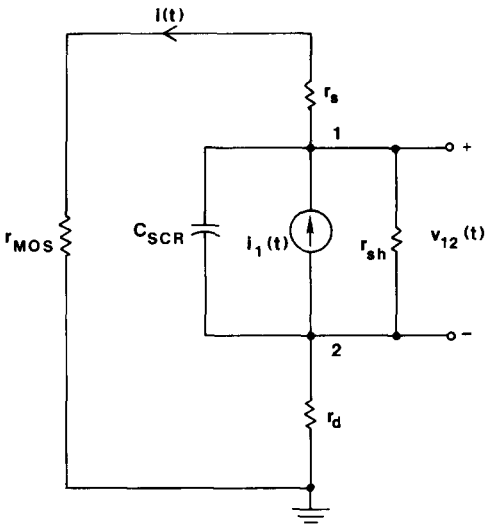

Fig. 5. Equivalent-circuit representation of the measurement circuit of Figs. 3 and 4 when the first-mode current dominates short-circuit current decay.

frequency current. In Fig. 5, r_s and r_{sh} are the series and shunt resistance of a solar cell, r_d detects the discharging current, and $i_1(t)$ is the first-term natural-frequency current.

The current $i(t)$ flowing through r_d in Fig. 5 is

$$i(t) = C_{SCR}\frac{dv_{12}(t)}{dt} + \frac{v_{12}(t)}{r_{sh}} + i_1(t) \tag{16}$$

where

$$C_{SCR} \equiv \frac{dQ_{SCR}}{dv_{12}(t)} = f\{v_{12}(t)\} \tag{17}$$

in which Q_{SCR}/e is the integrated steady-state hole or electron density through the volume of the space charge region. From Chawla and Gummel [6]

$$\frac{C_{SCR}}{C_{SCRO}} = \left(1 - \frac{v_{12}(t)}{V_g}\right)^{-m} \tag{18}$$

where C_{SCRO} is the C_{SCR} for variations in $v_{12}(t)$ about bias voltage $v_{12}(t) = 0$ and where $1/3 < m < 1/2$ and V_g is the gradient voltage [6], which includes the contribution of mobile holes and electrons within the space-charge region. Since $V_g \gg v_{12}(t)$,

$$C_{SCR} \approx C_{SCRO} \neq f\{v_{12}(t)\} \tag{19}$$

Thus

$$i(t) \approx C_{SCRO}\frac{dv_{12}(t)}{dt} + \frac{v_{12}(t)}{r_{sh}} + i_1(t) \tag{20}$$

where

$$v_{12}(t) = -(r_{MOS} + r_s + r_d)i(t) \tag{21}$$

Since the ratio $(r_{MOS} + r_d + r_s)/r_{sh}$ is usually very small for practical solar cells, we obtain from eqn. (20)

$$i(t) = -C_{SCRO}(r_{MOS} + r_s + r_d)\frac{di(t)}{dt} + i_1(t) \tag{22}$$

Solving eqn. (22) for $i(t)$ yields

$$i(t) = E_1 \exp\left(\frac{-t}{\tau_{SCR}}\right) + E_2 \exp\left(\frac{-t}{\tau_d}\right) \tag{23}$$

where

$$\tau_{SCRO} \equiv C_{SCRO}(r_{MOS} + r_s + r_d) \tag{24}$$

As can be seen in eqn. (23), the first term of the right-hand side can be neglected and τ_d can be determined if the time constant τ_{SCR} is much smaller than τ. For the switching circuit of Fig. 4, $\tau_{SCR} \approx 200$ ns. For the solar cells described in this paper, $0.5\ \mu s < \tau_d < 30\ \mu s$. Thus the time constant of the measurement circuit negligibly influences the first-term, or dominant natural-frequency, current decay of the solar cells.

3.3. Measurement of the dark current–voltage characteristics

The measurement of the dark I–V characteristics of a solar cell is straightforward. One first measures the terminal I–V_{out} characteristics in the dark condition and then corrects for the effects arising from the existence of the series resistance.

This method is based on the assumption that the main deviation of the diode current from the ideal $\exp(qV/kT)$ behavior at high currents can be attributed solely to series resistances [7].

From combining the measured I–V_{out} characteristic with idealized diode theory, we obtain

$$(V_{out})_i = I_i r_s + \frac{kT}{q}\ln\left(\frac{I_i}{I_{FO}}\right) \tag{25}$$

where r_s is the series resistance, I_{FO} is the idealized pre-exponential current (corresponding to unity slope), and the subscript i denotes different data points. Applied to two such data points, eqn. (25) yields

$$\Delta V_{out} = r_s \Delta I + \left(\frac{kT}{e}\right)\ln\left(\frac{I_2}{I_1}\right) \tag{26}$$

upon subtraction. This determines r_s, which we may thus ignore in the subsequent discussion.

In many cells the determination of I_{FO} is difficult because of the space-charge region and shunt currents. We can then determine r_s from the dark and $I_{sc}-V_{oc}$ characteristics [8].

3.4. Experimental results and discussion

In the most general case, the ratio X_{QNB}/L is arbitrary. For this case, we generated the $S(\tau)$ locus corresponding to the measured value of the decay time constant τ_d. This locus is generated by solving the transcendental equation B3 in Appendix II of ref. 1.

We consider the following ratios, for reasons that will become apparent

$$R = \frac{I_{FMO}}{I_{QNBO}} = f_1(S, \tau) \tag{8}$$

$$R_I = \frac{I_{QNEO}}{I_{QNBO}} = \frac{I_{FO} - I_{QNBO}}{I_{QNBO}} \tag{27}$$

$$R_M = \frac{I_{FMO}}{I_{FO}} \tag{15}$$

The relation among these parameters is

$$R = (1 + R_I)R_M \tag{28}$$

The ratio R is determined by theory for any assumed values of S and τ lying on the $S(\tau)$ locus corresponding to the measured value of the decay time constant τ_d. The ratio R_I is determined by the measured value of I_{FO} and by the value of I_{QNBO} which is obtained from eqn. (7) for any assumed values of S and τ. The ratio R_M is determined by measurement. Thus eqn. (28) enables a determination of S and τ by an iterative procedure.

To determine R_M, we use the ESCCD method as discussed in connection with eqn. (15) to determine the ratio (not the individual components of the ratio).

Having formed the three ratios above by a combination of experiment and theory, we search for the values of S and τ that satisfy eqn. (28). Completion of this search yields the actual values of S and τ for the solar cell under study. It also yields the ratio of the emitter to the base components of the total current, and hence these components separately if the base doping concentration is determined in the usual manner.

As an illustrative example, we consider a particular cell fabricated on a 0.3 Ω cm p-type substrate. The top n^+ layer is about 0.3 μm deep. The front surface is texturized and covered with an antireflective coating. The back surface has been implanted with boron. The concentration of boron is about 10^{20} cm^{-3} and the junction depth is 1 μm. The thickness of the base is 374 μm.

The measured values of τ_d, R_M and I_{FO} are 6.5 μs, 0.23 and approximately 2 pA respectively. Using $\tau_d = 6.5$ μs, we generate the $S(\tau)$ locus shown in Fig. 6. From this locus, we determine the values, 15 μs and

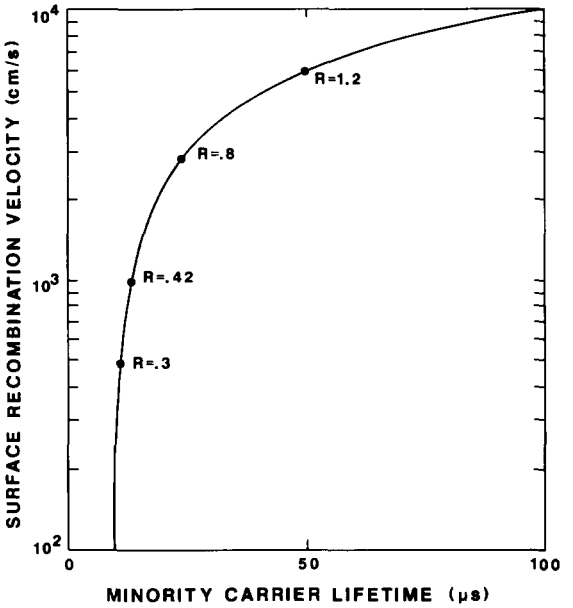

Fig. 6. $S(\tau)$ locus for a BSF 0.31 Ω cm n^+–p–p^+ solar cell. The locus is generated from $\tau_d = 6.5$ μs.

1300 cm s^{-1}, for the lifetime and the surface recombination velocity. The other parameters of this cell are also determined: $I_{QNBO} \approx 1$ pA, $I_{QNEO} \approx 1$ pA, $I_{FMO} \approx 0.46$ pA and $L \approx 185$ μm. The ratio of the cell thickness to the diffusion length is approximately 2 for this particular cell.

Such a solar cell has moderate thickness in the sense that, in the ESCCD transient, the minority carriers vanish from volume recombination and from exiting the front surface of the quasi-neutral base at comparable rates. To sharpen this definition of a moderately thick solar cell, we note that one can express the decay time constant τ_d in terms of the following two time constants by solving eqn. (A3) in Appendix A of ref. 1

$$\tau_d^{-1} = -s_1 = \tau_s^{-1} + \tau^{-1} \tag{29}$$

where $\tau_s = (X_{QNB}/A_1)^2/D$. Equal rates occur if

$$\tau_s = \tau \tag{30}$$

Here A_1 is obtained from eqn. (A3) of Appendix A

$$A_1 = \frac{\pi}{2} \quad \text{for } S(\text{back}) = 0 \tag{31}$$

and

$$A_1 = \pi \quad \text{for } S(\text{back}) = \infty \tag{32}$$

Here in eqn. 29, the parameter τ_d/τ_s is the probability that a minority carrier vanishes through the surfaces bounding the quasi-neutral region, whereas the parameter τ_d/τ is the probability that a minority carrier vanishes by volume recombination.

Although one will not know X_{QNB}/L for any given solar cell at the outset, X_{QNB} can be easily measured, and one can make an initial estimate of L as a function of the base doping concentration from past experience.

If $X_{QNB}/L \ll 1$, the procedure simplifies because the locus $S(\tau)$ exhibits $dS/d\tau \approx 0$ over a large range of τ. This is the mathematical statement, for our procedure, that S is more accurately determined than is τ for a thin-base solar cell. (If $X_{QNB}/L \gg 1$, $dS/d\tau \approx \infty$ over a large range of S, which means that τ is more accurately determined than is S for a long-base solar cell.)

To illustrate the procedure for thin solar cells, we consider two different n^+–p–p^+ BSF solar cells. These cells are fabricated on 10 Ω cm p-type substrates. The top n^+ layer is about 0.3 μm deep. The thickness of these cells is about 100 μm.

Using τ_d, we generate $S(\tau)$ loci of the two cells as shown in Fig. 7. For the cells corresponding to the lower and the upper loci, the actual values of S are estimated to be less than 190 cm s^{-1} and less than 3000 cm s^{-1} respectively. These maximum values (190 and 3000 cm s^{-1}), obtained from the region of the loci for which $dS/d\tau$ approaches zero, define S_{max}. If for an extreme case for which negligible volume recombination occurs during the ESCCD transient, $S = S_{max}$.

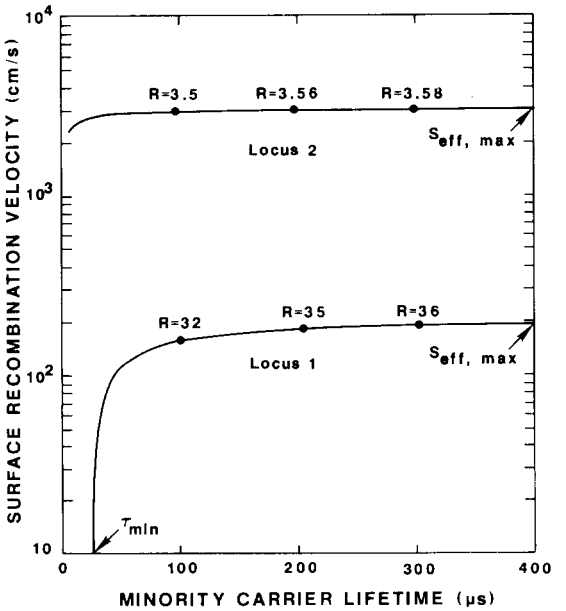

Fig. 7. $S(\tau)$ for two different solar cells with thin basewidth: locus 1, 10 Ω cm n^+–p–p^+ BSF solar cell with $X_{QNB} = 91$ μm and $\tau_d = 0.92$ μs; locus 2, 10 Ω cm n^+–p–p^+ BSF solar cell with $X_{QNB} = 101$ μm and $\tau_d = 74$ μs.

Similarly, the limit $dS/d\tau \to \infty$ defines a minimum value of the lifetime τ_{min}, as illustrated in Fig. 7. For all points corresponding to the lower locus of Fig. 7, $\tau_{min} \approx 40$ μs. This value τ_{min} occurs for the extreme case of negligible surface recombination at the back contact during the ESCCD transient. For the upper-locus cell in Fig. 7, $\tau_{min} \approx 0$. These two parameters, S_{max} and τ_{min}, can be used as performance parameters for thin solar cells; small S_{max} and large τ_{min} are desirable for thin BSF solar cells for a given base thickness and doping concentration.

We also measured the values of R_M: $R_M \approx 30$ for the lower locus and $R_M \approx 3$ for the upper locus. But we cannot use the measured R_M directly to determine τ, because R does not change much as τ increases, as is illustrated by marks on the loci of Fig. 7. Instead, the measured R_M can be used as another performance parameter for thin BSF solar cells, since large R_M means small I_{QNEO} and small S for a thin solar cell. These conditions imply a large open-circuit voltage for a given base thickness and doping. Small R_M usually implies either a poor BSF contact at the back surface or a large I_{QNEO}. For example, for the better BSF solar cell (the lower locus), we have $R_M \approx 30$, whereas $R_M \approx 3$ for a poorer BSF solar cell (the upper locus).

We measured various kinds of solar cells and characterized them as shown in Table 1. Among the cells in Table 1, poly1 and poly2 have highly doped poly-Si layers on the back surface of the base. The value of S is estimated to be about 2000 cm s^{-1} for an n^+–p–p^+-poly-Si cell (poly1) and about 400 cm s^{-1} for an p^+–n–n^+-poly-Si cell (poly2). Thin cells are characterized in terms of τ_{min} and S_{max}.

3.5. Two-cell method

Finally, we present one more method to determine the recombination parameters of solar cells. In this method, one fabricates two different solar cells out of the same wafer, one BSF solar cell and one ohmic-contact solar cell. The ohmic-contact cell can also be obtained by removal of the BSF region by etching or lapping. This will ensure equal lifetimes in both cells. One first estimates the lifetime of the cells by measuring τ_d of the ohmic-contact solar cell and by using eqn. (31)

$$\tau_d^{-1} = \left(\frac{X_{QNB}}{\pi}\right)^2 D^{-1} + \tau^{-1} \tag{33}$$

Secondly, one measures τ_d of the BSF solar cell and generates the $S(\tau)$ locus on the same plot. Since the lifetimes of the two cells are the same, S of the BSF cell can be obtained from the corresponding $S(\tau)$ locus.

An illustrative example is shown in Fig. 8. In this example, we used a wafer which is 10 Ω cm and p type. The upper locus corresponds to the ohmic-contact cell. The lower locus corresponds to the BSF cell. The lifetimes of these cells are estimated to be about 200 μs and the recombination velocity of the BSF cell is estimated to be 2000 cm s^{-1}.

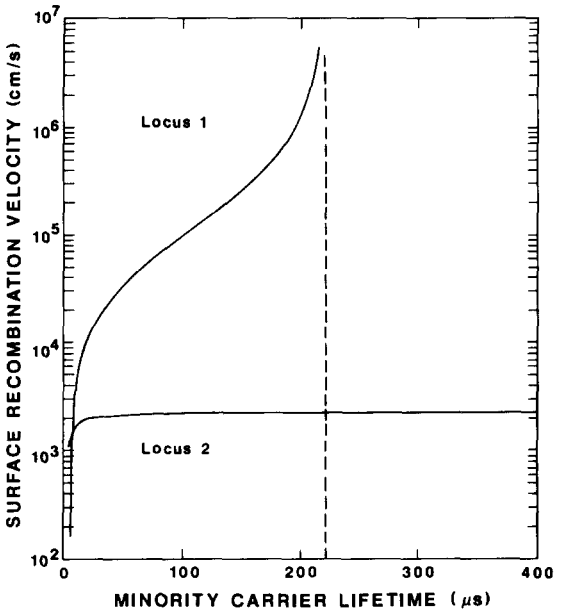

Fig. 8. Illustration of the determination procedure of S and τ using one ohmic contact solar cell and one BSF solar cell from the same material: locus 1, ohmic contact solar cell (C-3-5); locus 2, BSF solar cell (2-53).

TABLE 1

ESCCD measurements for various solar cells

Name	*Base resistivity* (Ω cm)	*Thickness* (μm)	τ_d (μs)	τ (μs)	S (cm/s)	L (μm)
SPIRE	0.31	374	6.5	15	1300	185
ASEC1	0.15	301	3.6	7	ohmic	93
ASEC2	0.15	267	4.0	13	ohmic	126
BSF1	10	240	5.3	35[b]	100 - 400[c]	350[b]
BSF2	10	260	6.3	45[b]	100 - 350[c]	400[b]
BSF3	10	284	7.85	75[b]	100 - 225[c]	512[b]
BSF4	10	96	0.98	20[b]	100 - 380[c]	265[b]
BSF5	10	91	0.9	25[b]	100 - 290[c]	295[b]
BSF6	10	107	0.7		4500[c]	
BSF7	10	102	0.73		3200[c]	
LEU1[a]	8	328	28.0	145[b]	40 - 80[c]	417[b]
LEU2[a]	1.5	325	25.7	105[b]	40 - 150[c]	347[b]
POLY1	2	203	2.7		2000[c]	
POLY2[a]	2	208	8.8	25[b]	100 - 400[c]	168[b]

[a] p^+–n–n^+ BSF solar cell.
[b] τ_{min} or L_{min}.
[c] S_{max}.
POLY1 and POLY2 have poly-Si layers on the back surfaces of the bases.

The error in τ introduced by error bounds on the measured thickness increases when the ratio X_{QNB}/L decreases. For example, for a 10 Ω cm n^+–p–p^+ solar cell (ohmic contact) with a thickness of 350 ± 3 μm, the error in the lifetime is estimated to be about 20%. In doing this calculation, we assumed that the lifetime is 50 μs ($X_{QNB}/L = 0.84$) and that $D = 35$ cm^2 s^{-1}. For a 0.3 Ω cm n^+–p–p^+ solar cell (ohmic contact) with a thickness of 350 ± 3 μm, this error is estimated to be about 5%. Here for this calculation, we assumed that the lifetime is 20 μs ($X_{QNB}/L = 1.64$) for diffusivity D = 23 cm^2 s^{-1}.

4. Discussion

For silicon solar cells, ESCCD has advantages over other methods for determining τ and S. The improvements of the theory and the experimental configurations presented here, together with the variations in the method, are meant to increase the practical utility of ESCCD.

Acknowledgments

A contract from the Jet Propulsion Laboratory helped support this work. We thank M. Spitzer and P. Iles for discussions and devices.

References

1 T. W. Jung and F. A. Lindholm, *IEEE Trans. Electron Devices, 31* (1984) 588.
2 J. G. Linvill and J. F. Gibbons, *Transistors and Active Circuits*, McGraw-Hill, New York, 1961.
3 W. C. Elmore, *J. Appl. Phys., 19* (1948) 55 - 63.
4 R. W. Dutton and R. J. Whittier, *IEEE Trans. Electron Devices, 16* (1969) 458 - 467.
5 S. M. Sze, *Physics of Semiconductor Devices*, Wiley, New York, 1981.
6 B. R. Chawla and H. K. Gummel, *IEEE Trans. Electron Devices, 18* (1971) 178 - 195.
7 T. H. Ning and D. D. Tang, *IEEE Trans. Electron Devices, 31* (1984) 409 - 412.
8 J. A. Mazer, A. Neugroschel and F. A. Lindholm, *IEEE Trans. Electron Devices, 28* (1981) 1530 - 1534.

Appendix A: Nomenclature

C_{SCR}	space-charge region capacitance
C_{SCRO}	C_{SCR} at $V = 0$
D	diffusion coefficient
D_p	hole diffusion coefficient
e	electronic charge
E_1, E_2	pre-exponential constants
$i_{first\text{-}mode}(0^+)$	initial amplitude of the first-mode current

$i(t)$	short-circuit transient current
$i_1(t)$	first-mode transient current
I	total dark terminal current
I_D	diode current in the dark
$I_F(0^-)$	forward steady-state current at $t = 0^-$
I_{FO}	steady-state forward saturation current
I_{FMO}	pre-exponential factor of the first natural-frequency current at $t = 0^-$
I_{QNBO}	base saturation current
I_{QNE}	emitter current
I_{QNEO}	emitter saturation current
I_{sc}	steady-state short-circuit current
I_{sh}	shunt current
k	Boltzmann constant
L	diffusion length
L_p^*	hole diffusion length for a.c. excitation
n_i	intrinsic density
N_{DD}	donor impurity density
Q_{SCR}	space charge region charge
r_d	load resistor
r_s	series resistance of a diode
r_{sh}	shunt resistance of the cell
R	I_{FMO}/I_{QNBO}
R_I	I_{QNEO}/I_{QNBO}
R_M	I_{FMO}/I_{FO}
s	Laplace transform variable
s_1	natural frequency for the first mode
S	surface recombination velocity
S_{max}	upper limit of S
t	time
T	absolute temperature (K)
V	forward voltage across the space charge region
$V(0^-)$	forward bias at $t = 0^-$ during transient
V_g	gradient voltage of a p–n junction
V_{oc}	open-circuit voltage
V_{out}	output voltage in dark
X_{QNB}	width of the quasi-neutral base

Greek symbols

α	ratio of recombination velocity S to diffusion velocity D/L
τ	minority carrier lifetime
τ_d	decay time constant
τ_{min}	lower limit of τ
τ_p	hole lifetime
τ_{SCR}	characteristic space charge region time constant
τ_{SCRO}	τ_{SCR} at $V = 0$